

Heat conduction of multilayer nanostructures with consideration of coherent and incoherent phonon transport

Bin Liu¹, Yangyu Guo², Vladimir I. Khvesyuk¹, Alexander A. Barinov¹, and Moran Wang³ (✉)

¹ Department of Thermophysics, Bauman Moscow State Technical University, Moscow 105005, Russia

² Institut Lumière Matière, Université Claude Bernard Lyon 1-CNRS, Université de Lyon, Villeurbanne 69622, France

³ Key Laboratory for Thermal Science and Power Engineering of Ministry of Education and Center for Flexible Electronics Technology, Tsinghua University, Beijing 100084, China

© Tsinghua University Press 2022

Received: 14 April 2022 / Revised: 13 May 2022 / Accepted: 22 May 2022

ABSTRACT

We report a theoretical investigation of coherent-to-incoherent heat conduction in multilayer nanostructures. In the coherent regime where the phonon motion is quasi-harmonic, the elastic continuum model gives accurate cross-plane thermal conductivity predictions of upper limits and demonstrates that the coherent transport is the result of the interplay between intrinsic wave effects. As the temperature or system size increases, the phonon dephasing scattering results in the deviation of thermal conductivity from the coherent-limit calculation. By further introducing the incoherence of phonons, we reproduce the classical minimum thermal conductivity, indicating the feasibility of extending the pure wave model into the wave-particle crossing regime.

KEYWORDS

GaAs/AlAs superlattices, thermal conductivity, coherent and incoherent phonon transport, continuum model

1 Introduction

Phonon thermal transport via nano-metamaterials has been extensively studied due to the potential of thermal design and thermoelectric-based energy conversion [1–3]. The artificial structures with periodic interfaces cause interference of phonons and control their coherent transport [4–9]. Multilayer nanostructures or superlattices (SLs) are ideal model systems for exploring and understanding the coherent-to-incoherent transition [10]. The coexistence of coherent and incoherent transport within the material exhibits the wave-particle duality of phonons. In these systems, coherent transport preserves the phase of phonons as they propagate through multiple interfaces, and has been observed mostly at low temperatures [11, 12]. The phase-destroying processes always start with mid- and high-frequency phonons excited at elevated temperatures, as they generally lose their phase correlation by interface diffuse scattering, internal elastic and inelastic scattering processes [13, 14]. Moreover, as the total length of the multilayer nanostructure increases, the coherence of low-frequency phonons could be dispersed at the system boundary or destroyed by long-range disturbances [4, 15].

One of the important characteristics of the coherent-to-incoherent transition is the existence of a minimum cross-plane thermal conductivity κ_{\perp} as a function of SL period thickness, which has been observed experimentally [10, 16, 17]. Numerous theoretical and simulation methods have been developed to interpret this phenomenon [18–22]. For instance, particle-based techniques such as Boltzmann transport equation [23–26], and Monte Carlo method [27, 28], have been extended to explain the wave interference effect of phonons in SLs [10]. While the

particlelike (or incoherent) picture has been extensively studied, direct descriptions of the wavelike (or coherent) transport are not readily available. The elastic continuum model naturally captures the intrinsic wave effects of phonons in acoustic metamaterials [29]. In addition to the interference effect, acoustic phonons with large wave vectors k may partially penetrate the thin films [30, 31], where energy is transferred by virtual phonons with imaginary k and decays exponentially [32]. This evanescent-wave based transfer is often termed as phonon tunneling [33–35]. For the oblique incidence, the longitudinal and transverse acoustic phonons are no longer independent due to the mode conversions occurring at the interfaces of metamaterials [36, 37]. The continuum model cannot accurately explain the heat transfer dominated by terahertz phonons with anharmonic scattering. However, the potential of the continuum model to describe the quasi-harmonic phonon thermal transport in the coherent regime remains to be developed. Meanwhile, the inclusion of incoherent effects into the continuum model remains challenging.

In this study, we demonstrate the accuracy of the continuum model describing the thermal transport of wavelike phonons in the coherent limit. Our predictions of κ_{\perp} for GaAs/AlAs SLs illustrate the significance of intrinsic wave interference, tunneling, and mode conversion effects. Ignoring the phonon dephasing that might be caused by interface scattering, we analyze the influence of interfacial roughness and mixing on both interfacial thermal conductance (ITC) at a single interface and coherent thermal transport in the SL. Due to the excitation of mid- and high-frequency phonons at high temperatures and the increase in the anharmonicity of long-period systems, the κ_{\perp} measured in this regime is lower than the continuum-model prediction [12]. By

Address correspondence to mrwang@tsinghua.edu.cn

further introducing the incoherence of phonons, we reproduce the classical minimum κ_{\perp} , indicating the feasibility of extending the pure wave model into the wave-particle crossing regime.

2 Method and computational details

The mean free path or wavelength of thermal phonons that dominate low-temperature heat transfer is much longer than the period thickness of SLs, the internal scattering of phonons that may result in the phase breaking becomes negligible. Meanwhile, if the interface is sharp enough, the phonon-interface scattering is specular. In this case, phonons can be quantified as elastic or acoustic waves. In this purely coherent regime, the lattice vibration that leads to the thermal conduction can be represented by harmonics and we describe the coherent transport of phonon waves by a continuum model.

The linear elasticity theory implies the existence of three modes of plane waves: two types of transverse waves, that are distinguished by whether the vibration direction is parallel to the reflecting interface, and one longitudinal wave, i.e., shear-horizontal (SH), shear-vertical (SV), and pressure (P) waves [38, 39]. Considering the wave propagation in the multilayer structure (Fig. 1), an incident wave will be reflected and transmitted multiple times in each layer. Due to the same exponential factor of all the forward waves in the same medium, they can be summarized into a resultant wave with an undetermined amplitude. Similarly, we have a backward resultant wave. Assuming that all the materials are isotropic, an independent P (or SV) wave incident on the interface will generate reflected P and SV waves, as well as transmitted P and SV waves. Considering this mode conversion effect, the incident P (or SV) wave has four resultant waves in each layer, as shown in Fig. 1.

The amplitude of each resultant wave is determined by the interfacial boundary conditions [39]. When no surface wave exists at the interface, the tangential components of the displacements and stresses are continuous across the interface. The transfer matrix method is commonly used to relate the amplitudes of waves between two different points inside the multilayer structure [36, 40, 41].

Consider the simple case of the SH wave incident on an N-period SL (see Fig. S1 in the Electronic Supplementary Material (ESM) for details). The tangential displacement $U_{j,n}(z) = A_{j,n}e^{ik_z z}$ and stress $S_{j,n}(z) = \mu_n \partial U_{j,n} / \partial z$ along the z -axis of propagating waves are continuous at each interface $z = z_n$, where the polarization mode of the wave $j = tS$ and rS , the first letter represents the excited wave (transmitted or reflected) and the second letter represents its polarization; k_z is the component of the wave vector in the z -coordinate direction; μ_n is the Lamé constant [39], and $n = 1, 2, \dots, 2N + 1$. The amplitudes of the resultant transmitted and reflected SH-waves in the n th layer, $A_{tS,n}$ and $A_{rS,n}$, can be defined by a column vector

$$w_n = \begin{bmatrix} A_{tS,n} \\ A_{rS,n} \end{bmatrix} \quad (1)$$

and the continuity conditions of the displacement and stress at the interfaces from z_{2N+1} to z_1 are expressed as

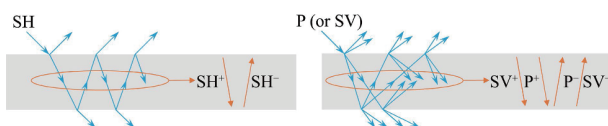


Figure 1 Schematic of SH, SV, and P wave propagation in each layer of the multilayer structure. In the continuum model, all waves generated in the layer are superimposed into corresponding forward (+) and backward (−) resultant waves.

$$H_{2N+2}(z_{2N+1}) w_{2N+2} = H_{2N+1}(z_{2N+1}) w_{2N+1}$$

$$H_{2N+1}(z_{2N}) w_{2N+1} = H_{2N}(z_{2N}) w_{2N}$$

⋮

$$H_3(z_2) w_3 = H_2(z_2) w_2$$

$$H_2(z_1) w_2 = H_1(z_1) w_1 \quad (2)$$

where the 2×2 matrix $H_n(z)$ is defined by

$$H_n(z) = \begin{bmatrix} e^{ik_z} & e^{-ik_z} \\ \mu_n k_z e^{ik_z} & -\mu_n k_z e^{-ik_z} \end{bmatrix} \quad (3)$$

From Eq. (2) we have the relation between w_1 and w_{2N+2}

$$w_1 = T w_{2N+2} \quad (4)$$

where $T = [H_1(z_1)]^{-1} H_2(z_1) \cdots [H_{2N+1}(z_{2N+1})]^{-1} H_{2N+2}(z_{2N+1})$ is the so-called transfer matrix [36]. Solution of Eq. (4) yields the amplitude ratio $A_{tS,1}/A_{tS,2N+2}$. The energy flux of the wave is given by

$$\eta_{j,n} = \frac{1}{2} \rho_n \omega^2 v_{g,j,n} A_{j,n}^2 \quad (5)$$

where ρ_n is the material density and $v_{g,j,n}$ is the group velocity [36]. Utilizing the transfer matrix method, it is convenient to calculate the transmissivity α_i of the SL system, which is defined as the proportion of incident-wave energy flow transmitted into the substrate. The transmissivity of the incident SH wave

$$\alpha_{SH} = \frac{\eta_{tS,1}}{\eta_{tS,2N+2}} \quad (6)$$

The transmissivity α_i is the decisive parameter of the thermal conductance G across a single interface or multilayer structure. The transmissivity of phonon waves is frequency dependent. In the calculation, the frequency spectrum of α_j is determined by introducing the phonon dispersions $\omega = \omega(k)$ of each constitute material in the system (Fig. S2 in the ESM), including the metal detection layer and substrate (or buffer layer). The thermal conductance of the SL G_{SL} is determined by applying the Landauer transport formalism [42, 43]. And the effective κ_{\perp} of the SL is computed by

$$\kappa_{\perp} = G_{SL} L \quad (7)$$

where L is the total length of the SL. Detailed model descriptions and calculations, including the incidence of P (or SV) wave, can be found in the ESM.

It is worth noting that as the angle of incidence exceeds the critical angle, the total internal reflection occurs at the interface between two semi-infinite or thick mediums [38, 39]. While for thin films, it has been proved that the contribution of tunneling carriers to energy transmission cannot be ignored [44, 45]. In addition, the partial intermixing that naturally occurs during growth may lead to the interface disorder (or roughness) and component mixing [12, 46]. Under the coherent limit where the dephasing caused by the mixing layer can be ignored, the influence of component mixing is attributed to the changes in the acoustic mismatch of two adjacent layers. Regarding the mixing layer as a separate layer with the average acoustic properties of the media on both sides [47], the transmissivity is directly obtained by the transfer-matrix calculation. Meanwhile, we exclude the interfacial mass-defect scattering due to its small effect on the transmission of long-wave phonons in the short-period SLs [48]. For materials with low lattice mismatch (e.g., GaAs/AlAs), the influence of mass defects and dislocations will be much smaller [49, 50]. The discontinuity at the interface will increase as the contrast between individual components of the unit cell are

enhanced. It also means that the phase destruction of phonons is more likely to exist at the boundaries of highly dissimilar materials.

3 Results and discussion

The fidelity of the continuum model is validated by comparing to the measured κ_{\perp} of a series of GaAs/AlAs SLs with a fixed period thickness $d_{\text{SL}} = 24 \text{ nm}$ [12], as shown in Fig. 2.

The linear relation between κ_{\perp} and the number of periods N (or the total length L , as d_{SL} is a constant) suggests the coherent thermal transport of phonons in these SLs. If phonons propagate by pure particle behavior, the κ_{\perp} of the SL with a fixed d_{SL} should be independent of N because each interface acts as a thermal resistor. The calculated results agree well with the measured κ_{\perp} in the pure coherent regime: as temperatures $T \leq 150 \text{ K}$ or SL is short-period ($N \leq 5$ periods), indicating a linearity of the κ_{\perp} vs. N . With the increase of the temperature or system size, the excitation of middle- and high-frequency phonons and the enhancement of interface diffuse scattering result in the dephasing of coherent phonons. The measured κ_{\perp} deviates from the coherent-limit calculation due to the anharmonicity of the SL system.

Despite of the coherent-limit consideration, it is still necessary to quantify the acoustic mismatch changes caused by the interfacial mixing. Here the interface mixing is treated as independent additional thin layers between adjacent layers. Phonons in the mixing layer are considered to maintain their phase and satisfy the interfacial boundary conditions. Figure S3 in the ESM shows the schematic of the SL system, where a mixing layer is added between every two adjacent GaAs and AlAs layers,

while N and L remain unchanged. Meanwhile, the number of periods of the SL becomes $2N$. In Fig. 2(a) the solid and dashed lines illustrate the κ_{\perp} of SLs with perfect and mixed interfaces, respectively. The results indicate that the mixing layers reduce the mass difference and acoustic mismatch between alternating GaAs and AlAs layers, resulting in a reduction of the interfacial thermal resistance and a slight increase of κ_{\perp} .

Moreover, we quantify the influence of intrinsic wave effects on coherent thermal transport. The inset in Fig. 2(b) shows the important contributions of tunneling phonons and the differences between SH, SV, and P modes at 150 K. Despite the high transmissivity of longitudinal P-waves, their smaller density of states reduces their contribution to κ_{\perp} , which is smaller than the κ_{\perp} of shear waves. As the angle of incidence θ_i is greater than the critical angle θ_c , the total internal reflection occurs at the interface and confines the propagation of phonon waves. Due to the mode conversion effect, the transmission channel (SV-SV and SV-P transmission) and the possible number of θ_c of SV wave are more complicated than those of SH wave. For instance, as $\theta_i \leq \theta_c$, a small fraction of the SV incident wave is converted into P wave, resulting in the critical incident angle being reached quickly. Therefore, the confinement effect of total internal reflection on the two shear waves is different and leads to their different contributions to κ_{\perp} .

In order to better illustrate the above results and quantify the phonon interference effect, Fig. 3 shows the angle- and frequency-dependent phonon transmissivity of short-period GaAs/AlAs SLs, comparing with that of a single GaAs/AlAs interface. For the elastic scattering process of phonon waves, the transmissivity is independent of temperature. In Fig. 3, phonon waves with small θ_i have higher transmissivity, while they are strongly reflected when θ_i reaches the glazing angle or 90° . For the SL samples under consideration [12], owing to the highest longitudinal velocity in the incident medium (aluminum), the incident P waves transmit across the system without any critical angle θ_c . The vertical discontinuities in the SV and SH contour plots are caused by the critical angle θ_c . Due to the mode conversion, SV wave has two critical angles $\theta_{c,1}$ and $\theta_{c,2}$, while SH wave only has one θ_c . For incident SV waves, in the range of angles $\theta_{c,1} < \theta_i < \theta_{c,2}$, the transmitted P wave is transformed into a surface wave at the interface and partially tunnels across the next layer. The “tunneling I” in the plot is a single-mode tunneling. Above the second transverse-mode critical angle $\theta_i > \theta_{c,2}$, the next layer can support two modes (both P and SV) of tunneling phonons and the second tunneling region is multimode tunneling.

Obviously, compared with the transmissivity of a single GaAs/AlAs interface, the transmissivity of SLs becomes lower and forms several bandgaps, indicating the phonon interference effect in SLs. Tunneling phonons are also influenced by the periodic structure and exhibit the interference effect. The confinement caused by the total internal reflection and interference effect can effectively reduce the heat conductance of SLs, while tunneling of phonon waves causes a moderate recovery of the heat conductance. This implies that various wave mechanisms participate in the phonon coherent transport of SLs and play significant roles. These detailed analyses contribute to the understanding of coherent transport behavior of phonons. However, it is clear that the continuum model with the harmonic assumption cannot capture the particlelike behavior of phonons. In Fig. 2, the calculated κ_{\perp} by the coherent-limit model will continuously rise and diverge as d_{SL} increases [14]. In addition, the classical minimum κ_{\perp} due to the competition between coherent and incoherent transport cannot be estimated by the continuum model [10].

Further, we introduce the internal and interface scatterings of

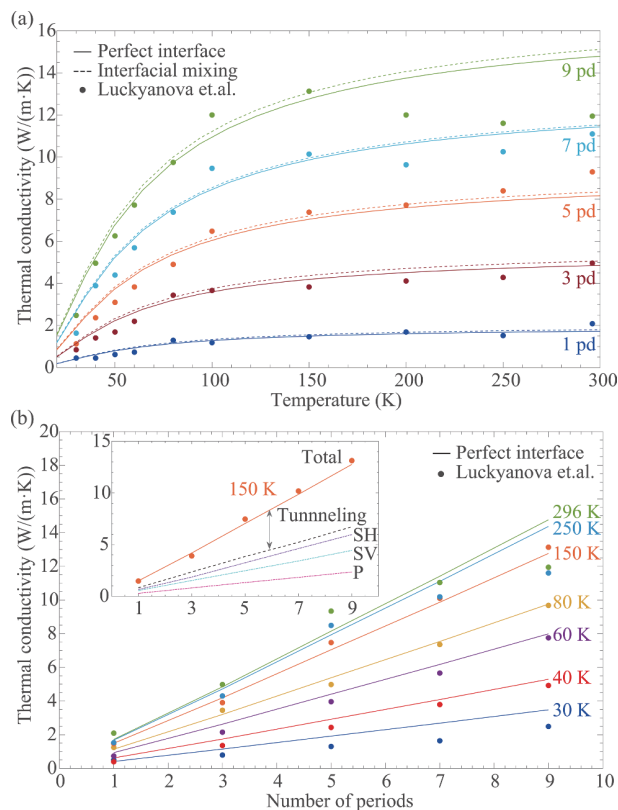


Figure 2 (a) Calculated and measured κ_{\perp} vs. the temperature of GaAs/AlAs SLs with a fixed period thickness [12]. The calculated κ_{\perp} increases due to the acoustic mismatch reduction caused by interfacial mixing. (b) Calculated and measured κ_{\perp} vs. the number of periods of GaAs/AlAs SLs. The inset shows the contributions of SH, SV, and P polarization modes to the total κ_{\perp} at 150 K, whereas the dashed line indicates the calculated κ_{\perp} without the contribution of tunneling phonons.

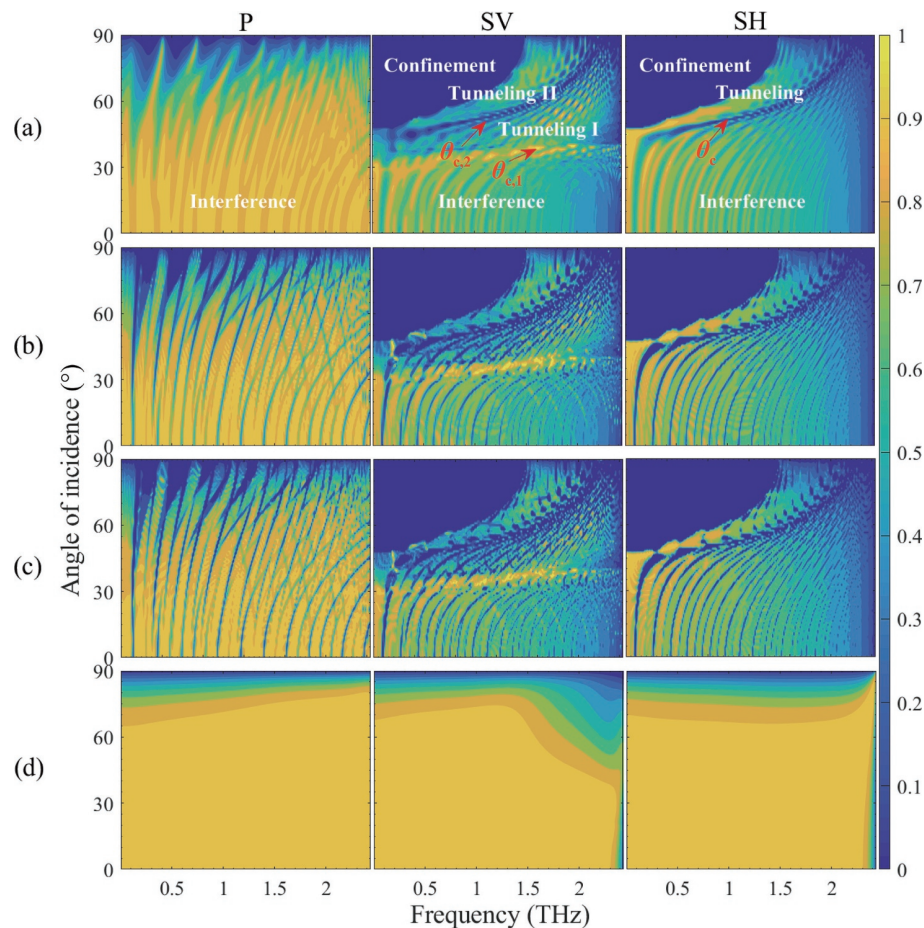


Figure 3 Transmissivity as a function of the frequency and angle of incidence of P, SV, and SH polarized phonon waves in GaAs/AlAs SLs with (a) 1, (b) 3, (c) 5 periods, and (d) at a single GaAs/AlAs interface. When the angle of incidence reaches the critical angle θ_c , the total internal reflection and phonon tunneling occur at the interface.

phonons to consider the role of incoherent transport. The transport regimes are determined by the comparison between the SL characteristic size (i.e., the period thickness) and the relevant length of different phonon scattering processes. The distinction between the coherent and incoherent phonons is still under debate as the wavelike behavior of phonons is more related to coherence length and wavelength [14, 51, 52], while the widely used mean free path usually determines their particlelike behavior. Here we simply use the wavelength of plane waves, which separates the specular and diffuse scattering at the interface, to qualitatively distinguish the coherent and incoherent phonons [39]. The incoherent transport calculation is based on the Boltzmann transport model, and the thermal conductivity of each layer is computed by the Holland–Callaway model with input from the first principles results [53–56], while the ITC is calculated by an interfacial continuum model [57] (see the ESM for more details). By combining the contributions of coherent and incoherent phonons, the effective G_{SL} and κ_{\perp} are obtained. In Fig. 4, we observe the minimum κ_{\perp} in the coherent–incoherent transition regime, which has been observed in experiments with other materials [10, 16, 51]. Despite the simplified assumptions used in the above calculation, the continuum model exhibits the potential to describe the wave–particle crossing of phonons.

With an improved description of the wave scattering at a single interface, here we also investigate the ITC by the continuum model. The elastic thermal transport of phonons dominates the ITC at considered temperatures [58]. The linear elasticity theory assumes the wave specular scattering at the interface, which is only applicable in the coherent regime where the wavelength of dominant phonons is much longer than the interface defects.

While incoherent phonons are easily diffusely scattered by the imperfect interface, which cannot be neglected. We assume that the interface defects or irregularities transfers to the interfacial roughness [16]. Using a Gaussian-distributed statistically rough interface and the Kirchhoff approximation [59–61], we introduce the interface diffuse scattering of phonon waves into the continuum model and verify its feasibility of predicting the ITC (Fig. S4 in the ESM). In addition, the presented results of ITC and other experiments indicate that even at high temperatures, sub-nanometer roughness has only a weak effect on the transmissivity of mid- to high-frequency phonons [62, 63]. However, it is worth noting that when the wavelike phonons are repeatedly scattered in long-period SLs, the randomization of the wave direction and the phase difference between waves by the interface diffuse scattering may also result in their phase breaking. This might be a significant factor for the κ_{\perp} deviation from coherent transport in Fig. 2, and should be the focus of further coherent-to-incoherent research.

4 Conclusions

In conclusion, the elastic continuum model well predicts the thermal conductivity κ_{\perp} of multilayer nanostructures in the coherent limit, which is the result of the interplay between intrinsic wave effects (i.e., interference, tunneling, and mode conversion effects). Additionally, our study unveils the effects of interfacial mixing and roughness on coherent thermal transport. We find that the interface diffuse scattering has a weak influence on the transmissivity of coherent phonons, and the calculated κ_{\perp} will diverge as the length of SLs increases in absence of other scattering mechanisms. However, the interface diffuse scattering

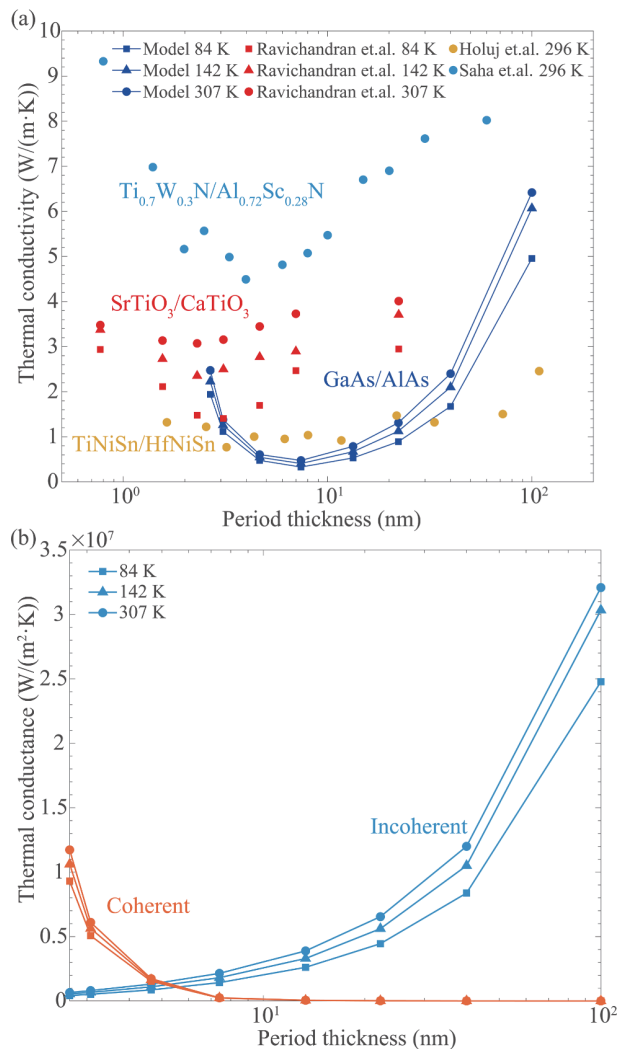


Figure 4 (a) Calculated κ_{\perp} vs. d_{SL} of GaAs/AlAs SLs with fixed total length $L = 200$ nm and the experimental results of other materials [10, 16, 51]. (b) Contributions of coherent and incoherent phonons to the thermal conductance G_{SL} across GaAs/AlAs SLs obtained by the presented model.

results in the phase randomization of phonons in the long-period SLs, resulting in the deviation of κ_{\perp} from the coherent limit. By further introducing the phonon internal and interface scatterings, we reproduce the classical minimum κ_{\perp} with varying superlattice period. The results presented indicate the feasibility of extending the pure wave model into the wave-particle crossing regime and contribute to the understanding and manipulation of phonon wave behaviors in nanostructures.

Acknowledgements

The authors thank the Tsinghua University Initiative Scientific Research Program for financial support.

Electronic Supplementary Material: Supplementary material (description of the elastic continuum model, computational details, phonon-interface scattering and other explanations) is available in the online version of this article at <https://doi.org/10.1007/s12274-022-4589-7>.

References

[1] Li, Y.; Li, W.; Han, T. C.; Zheng, X.; Li, J. X.; Li, B. W.; Fan, S. H.; Qiu, C. W. Transforming heat transfer with thermal metamaterials and devices. *Nat. Rev. Mater.* **2021**, *6*, 488–507.
 [2] Chowdhury, P. R.; Shi, J. J.; Feng, T. L.; Ruan, X. L. Prediction of

$\text{Bi}_2\text{Te}_3\text{-Sb}_2\text{Te}_3$ interfacial conductance and superlattice thermal conductivity using molecular dynamics simulations. *ACS Appl. Mater. Interfaces* **2021**, *13*, 4636–4642.

- [3] Ren, W. Y.; Li, H. D.; Gao, L.; Li, Y.; Zhang, Z. Y.; Long, C. J.; Ji, H. N.; Niu, X. B.; Lin, Y.; Wang, Z. M. Epitaxial growth and thermal-conductivity limit of single-crystalline $\text{Bi}_2\text{Se}_3/\text{In}_2\text{Se}_3$ superlattices on mica. *Nano Res.* **2017**, *10*, 247–254.
 [4] Nomura, M.; Anufriev, R.; Zhang, Z. W.; Maire, J.; Guo, Y. Y.; Yanagisawa, R.; Volz, S. Review of thermal transport in phononic crystals. *Mater. Today Phys.* **2022**, *22*, 100613.
 [5] Kuchuk, A. V.; De Oliveira, F. M.; Ghosh, P. K.; Mazur, Y. I.; Stanchu, H. V.; Teodoro, M. D.; Ware, M. E.; Salamo, G. J. Coherent-interface-induced strain in large lattice-mismatched materials: A new approach for modeling Raman shift. *Nano Res.* **2022**, *15*, 2405–2412.
 [6] Cai, C. Y.; Zhao, Y. H.; Chang, F. R.; Zhao, X. B.; Yang, L. T.; Liang, C. Y.; Wang, G. W.; Niu, Z. C.; Shi, Y.; Liu, X. H. et al. Understanding the role of interface in advanced semiconductor nanostructure and its interplay with wave function overlap. *Nano Res.* **2020**, *13*, 1536–1543.
 [7] Ma, D.; Arora, A.; Deng, S.; Xie, G.; Shiomi, J.; Yang, N. Quantifying phonon particle and wave transport in silicon nanophononic metamaterial with cross junction. *Mater. Today Phys.* **2019**, *8*, 56–61.
 [8] Yang, N.; Zhang, G.; Li, B. W. Ultralow thermal conductivity of isotope-doped silicon nanowires. *Nano Lett.* **2008**, *8*, 276–280.
 [9] Wu, X.; Han, Q. Transition from incoherent to coherent phonon thermal transport across graphene/h-BN van der Waals superlattices. *Int. J. Heat Mass Transf.* **2022**, *184*, 122390.
 [10] Ravichandran, J.; Yadav, A. K.; Cheaito, R.; Rossen, P. B.; Soukiasian, A.; Suresha, S. J.; Duda, J. C.; Foley, B. M.; Lee, C. H.; Zhu, Y. et al. Crossover from incoherent to coherent phonon scattering in epitaxial oxide superlattices. *Nat. Mater.* **2014**, *13*, 168–172.
 [11] Anufriev, R.; Maire, J.; Nomura, M. Review of coherent phonon and heat transport control in one-dimensional phononic crystals at nanoscale. *APL Mater.* **2021**, *9*, 070701.
 [12] Luckyanova, M. N.; Garg, J.; Esfarjani, K.; Jandl, A.; Bulsara, M. T.; Schmidt, A. J.; Minnich, A. J.; Chen, S.; Dresselhaus, M. S.; Ren, Z. F. et al. Coherent phonon heat conduction in superlattices. *Science* **2012**, *338*, 936–939.
 [13] Guo, Y. Y.; Bescond, M.; Zhang, Z. W.; Luisier, M.; Nomura, M.; Volz, S. Quantum mechanical modeling of anharmonic phonon-phonon scattering in nanostructures. *Phys. Rev. B* **2020**, *102*, 195412.
 [14] Latour, B.; Volz, S.; Chalopin, Y. Microscopic description of thermal-phonon coherence: From coherent transport to diffuse interface scattering in superlattices. *Phys. Rev. B* **2014**, *90*, 014307.
 [15] Tian, Y. L.; Puurtinen, T. A.; Geng, Z. R.; Maasilta, I. J. Minimizing coherent thermal conductance by controlling the periodicity of two-dimensional phononic crystals. *Phys. Rev. Appl.* **2019**, *12*, 014008.
 [16] Holuj, P.; Euler, C.; Balke, B.; Kolb, U.; Fiedler, G.; Müller, M. M.; Jaeger, T.; Angel, E. C.; Kratzer, P.; Jakob, G. Reduced thermal conductivity of TiNiSn/HfNiSn superlattices. *Phys. Rev. B* **2015**, *92*, 125436.
 [17] Saha, B.; Koh, Y. R.; Comparan, J.; Sadasivam, S.; Schroeder, J. L.; Garbrecht, M.; Mohammed, A.; Birch, J.; Fisher, T.; Shakouri, A. et al. Cross-plane thermal conductivity of (Ti, W)N/(Al, Sc)N metal/semiconductor superlattices. *Phys. Rev. B* **2016**, *93*, 045311.
 [18] Chen, Y. F.; Li, D. Y.; Lukes, J. R.; Ni, Z. H.; Chen, M. H. Minimum superlattice thermal conductivity from molecular dynamics. *Phys. Rev. B* **2005**, *72*, 174302.
 [19] Daly, B. C.; Maris, H. J.; Imamura, K.; Tamura, S. Molecular dynamics calculation of the thermal conductivity of superlattices. *Phys. Rev. B* **2002**, *66*, 024301.
 [20] Guo, Y. Y.; Bescond, M.; Zhang, Z. W.; Xiong, S. Y.; Hirakawa, K.; Nomura, M.; Volz, S. Thermal conductivity minimum of graded superlattices due to phonon localization. *APL Mater.* **2021**, *9*, 091104.
 [21] Schelling, P. K.; Phillpot, S. R. Multiscale simulation of phonon transport in superlattices. *J. Appl. Phys.* **2003**, *93*, 5377–5387.

- [22] Ravichandran, N. K.; Minnich, A. J. Coherent and incoherent thermal transport in nanomeshes. *Phys. Rev. B* **2014**, *89*, 205432.
- [23] Garg, J.; Chen, G. Minimum thermal conductivity in superlattices: A first-principles formalism. *Phys. Rev. B* **2013**, *87*, 140302.
- [24] Simkin, M. V.; Mahan, G. D. Minimum thermal conductivity of superlattices. *Phys. Rev. Lett.* **2000**, *84*, 927–930.
- [25] Ye, E.; Minnich, A. J. Ab initio based investigation of thermal transport in superlattices using the Boltzmann equation: Assessing the role of phonon coherence. *J. Appl. Phys.* **2019**, *125*, 055107.
- [26] Zhang, Z. W.; Guo, Y. Y.; Bescond, M.; Chen, J.; Nomura, M.; Volz, S. Heat conduction theory including phonon coherence. *Phys. Rev. Lett.* **2022**, *128*, 015901.
- [27] Li, Q.; Ye, W. J. An interfering monte carlo method for partially coherent phonon transport in superlattices. *Int. J. Heat Mass Transf.* **2017**, *107*, 534–543.
- [28] Yu, J. C.; Li, Q.; Ye, W. J. Investigation of wave interference effect in Si/Ge superlattices with interfering monte carlo method. *Int. J. Heat Mass Transf.* **2019**, *128*, 270–278.
- [29] Deymier, P. A. *Acoustic Metamaterials and Phononic Crystals*; Springer: Berlin, Heidelberg, 2013.
- [30] Budaev, B. V.; Bogy, D. B. Heat transport by phonon tunneling across layered structures used in heat assisted magnetic recording. *J. Appl. Phys.* **2015**, *117*, 104512.
- [31] Yang, S. X.; Page, J. H.; Liu, Z. Y.; Cowan, M. L.; Chan, C. T.; Sheng, P. Ultrasound tunneling through 3D phononic crystals. *Phys. Rev. Lett.* **2002**, *88*, 104301.
- [32] Mauranyapin, N. P.; Romero, E.; Kalra, R.; Harris, G.; Baker, C. G.; Bowen, W. P. Tunneling of transverse acoustic waves on a silicon chip. *Phys. Rev. Appl.* **2021**, *15*, 054036.
- [33] Brekhovskikh, L. M.; Godin, O. A. *Acoustics of Layered Media I: Plane and Quasi-Plane Waves*; Springer: Berlin, Heidelberg, 1990.
- [34] Jiang, X.; Shi, C. Z.; Li, Z. L.; Wang, S. Q.; Wang, Y.; Yang, S.; Louie, S. G.; Zhang, X. Direct observation of Klein tunneling in phononic crystals. *Science* **2020**, *370*, 1447–1450.
- [35] Tian, Z. T.; White, B. E.; Sun, Y. Phonon wave-packet interference and phonon tunneling based energy transport across nanostructured thin films. *Appl. Phys. Lett.* **2010**, *96*, 263113.
- [36] Tamura, S.; Hurley, D. C.; Wolfe, J. P. Acoustic-phonon propagation in superlattices. *Phys. Rev. B* **1988**, *38*, 1427–1449.
- [37] Yoshihiro, T.; Nishiguchi, N. Mode-conversion effects of phonons on Anderson localization. *Phys. Rev. B* **2019**, *100*, 235441.
- [38] Achenbach, J. D. *Wave Propagation in Elastic Solids*; Elsevier: Amsterdam, 1973.
- [39] Auld, B. A. *Acoustic Fields and Waves in Solids*; Wiley-Interscience: New York, 1973.
- [40] Chen, G. Phonon wave heat conduction in thin films and superlattices. *J. Heat Transf.* **1999**, *121*, 945–953.
- [41] Chen, G. *Nanoscale Energy Transport and Conversion: A Parallel Treatment of Electrons, Molecules, Phonons, and Photons*; Oxford University Press: Oxford, 2005.
- [42] Datta, S. *Electronic Transport in Mesoscopic Systems*; Cambridge University Press: Cambridge, 1995.
- [43] Swartz, E. T.; Pohl, R. O. Thermal boundary resistance. *Rev. Mod. Phys.* **1989**, *61*, 605–668.
- [44] Brekhovskikh, L. M.; Godin, O. A. *Acoustics of Layered Media II: Point Sources and Bounded Beams*; Springer: Berlin, Heidelberg, 1999.
- [45] Tsu, R.; Esaki, L. Tunneling in a finite superlattice. *Appl. Phys. Lett.* **1973**, *22*, 562–564.
- [46] Rajeev, A.; Chen, W. X.; Kirch, J. D.; Babcock, S. E.; Kuech, T. F.; Earles, T.; Mawst, L. J. Interfacial mixing analysis for strained layer superlattices by atom probe tomography. *Crystals* **2018**, *8*, 437.
- [47] Beechem, T.; Graham, S.; Hopkins, P.; Norris, P. Role of interface disorder on thermal boundary conductance using a virtual crystal approach. *Appl. Phys. Lett.* **2007**, *90*, 054104.
- [48] Liu, B.; Khvesyuk, V. I.; Barinov, A. A.; Wang, M. R. Effect of interfacial roughness on thermal boundary conductance: An elastic wave model using the Kirchhoff approximation. *Int. J. Mech. Sci.* **2022**, *218*, 106993.
- [49] Hepplestone, S. P.; Srivastava, G. P. Theory of interface scattering of phonons in superlattices. *Phys. Rev. B* **2010**, *82*, 144303.
- [50] Hepplestone, S. P.; Srivastava, G. P. Lattice dynamics and thermal properties of phononic semiconductors. *Phys. Rev. B* **2011**, *84*, 115326.
- [51] Saha, B.; Koh, Y. R.; Feser, J. P.; Sadasivam, S.; Fisher, T. S.; Shakouri, A.; Sands, T. D. Phonon wave effects in the thermal transport of epitaxial TiN/(Al, Sc)N metal/semiconductor superlattices. *J. Appl. Phys.* **2017**, *121*, 015109.
- [52] Latour, B.; Chalopin, Y. Distinguishing between spatial coherence and temporal coherence of phonons. *Phys. Rev. B* **2017**, *95*, 214310.
- [53] Callaway, J. Model for lattice thermal conductivity at low temperatures. *Phys. Rev.* **1959**, *113*, 1046–1051.
- [54] Holland, M. G. Analysis of lattice thermal conductivity. *Phys. Rev.* **1963**, *132*, 2461–2471.
- [55] Guo, Y. Y.; Wang, M. R. Lattice Boltzmann scheme for hydrodynamic equation of phonon transport. *Int. J. Therm. Sci.* **2022**, *171*, 107178.
- [56] Lindsay, L.; Broido, D. A.; Reinecke, T. L. Ab initio thermal transport in compound semiconductors. *Phys. Rev. B* **2013**, *87*, 165201.
- [57] Liu, B.; Khvesyuk, V. I. Analytical model for thermal boundary conductance based on elastic wave theory. *Int. J. Heat Mass Transf.* **2020**, *159*, 120117.
- [58] Koh, Y. R.; Shi, J. J.; Wang, B. W.; Hu, R. J.; Ahmad, H.; Kerdsonpanya, S.; Milosevic, E.; Doolittle, W. A.; Gall, D.; Tian, Z. T. et al. Thermal boundary conductance across epitaxial metal/sapphire interfaces. *Phys. Rev. B* **2020**, *102*, 205304.
- [59] Bass, F. G.; Fuks, I. M. *Wave Scattering from Statistically Rough Surfaces*; Elsevier: Amsterdam, 1979.
- [60] Ogilvy, J. A. Wave scattering from rough surfaces. *Rep. Prog. Phys.* **1987**, *50*, 1553–1608.
- [61] Shi, F.; Lowe, M.; Craster, R. Diffusely scattered and transmitted elastic waves by random rough solid-solid interfaces using an elastodynamic Kirchhoff approximation. *Phys. Rev. B* **2017**, *95*, 214305.
- [62] Duda, J. C.; Hopkins, P. E. Systematically controlling Kapitza conductance via chemical etching. *Appl. Phys. Lett.* **2012**, *100*, 111602.
- [63] Hopkins, P. E.; Duda, J. C.; Petz, C. W.; Floro, J. A. Controlling thermal conductance through quantum dot roughening at interfaces. *Phys. Rev. B* **2011**, *84*, 035438.